Primate Saccade Rhythmicity

Tim Näher[1,2*], Yufeng Zhang[1,2,3*], Martina Pandinelli[1,2] & Pascal Fries[1,2,3]

1 Ernst Strüngmann Institute (ESI) for Neuroscience in Cooperation with Max Planck Society, Frankfurt, Germany.

2 Donders Institute for Brain, Cognition and Behaviour, Radboud University, Nijmegen, Netherlands.

3 International Max Planck Research School for Neural Circuits, Frankfurt, Germany

* Contributed equally

Corresponding authors: tim.naeher@esi-frankfurt, yufeng.zhang@esi-frankfurt.de, pascal.fries@esi-frankfurt

Abstract

Active sensing behaviors in rodents display theta (4-8 Hz) rhythmicity. Whether similar rhythmicity exists in primate saccadic eye movements has remained a matter of debate. We studied saccade dynamics in 22 human participants and two macaque monkeys, examining the influence of different visual stimuli and tasks. Inter-saccadic intervals (ISIs) reliably revealed a characteristic duration and under certain conditions clear theta rhythmicity. Rhythmicity was strongest for saccades with short ISIs. Surprisingly, the degree of rhythmicity was not due to spatial regularity of the visual scene, but it was shaped by task demands. Macro- and micro-saccade ISIs shared similar characteristic durations. Naturally occurring micro-saccades provided evidence that ISIs can become more regular without becoming faster. During free-viewing, subsequent ISIs were not independent, but the visual system switched between states of low and high rhythmicity. Humans and macaques showed similar saccade dynamics, suggesting a potential common evolutionary trait in primate active visual sensing.

Significance Statement

Active sensing, wherein organisms deliberately orient their sensory organs to probe their environment, is a cornerstone of perceptual experience. While certain animals like rodents showcase rhythmic patterns in such behaviors, the presence of similar rhythms in primate vision remains contested. In our two-species study, involving human participants and macaque monkeys, we unveil a distinctive rhythmic pattern of saccades, the main visual sensing behavior of primates. Interestingly, this rhythm resonates with known theta rhythms. Notably, this rhythmicity was not necessarily determined by the visual scene but was modulated by the task at hand. Our findings shed light on a potentially shared evolutionary trait in primate vision, underscoring the intricate interplay between perception, action, and cognition.

Introduction

The continuous loop of action and perception is a fundamental process in organisms across the biological spectrum, stemming from their need to sense, interpret, and react to their surroundings [1]. Importantly, sensing is not confined to the passive reception of sensory information. Instead, it can involve deliberately reorienting the sensory organs through active control, a process called active sensing [2, 3]. Active sensing is prominently observed in primates during visual exploration, entailing frequent sampling eye movements, called saccades. Saccades shift the fovea, the central area of the retina with the highest visual acuity , to parts of the visual scene, thereby sequentially taking high-resolution samples from the surrounding [4]. This active segmentation process reflects how the brain's neural networks handle complex multi-element inputs, namely by selecting one element at a time for deep processing [5-8]. The multi-layer processing implemented in our hierarchically organized visual

recognition system likely requires this temporal parsing, such that active sensing might not merely be an operational preference but an implementational requirement [9].

During natural exploration, the foveated part of the scene is typically the focus of attention [10]. Consequently, shifts of the fovea through saccadic eye movements are expressions of shifts in overt attention. These shifts typically occur with characteristic inter-saccadic intervals (ISIs), showing a unimodal ISI distribution with a clear peak [11]. The ISIs (minus the saccadic flight times) reflect the durations the visual system spends on processing the respective foveated segments. Intriguingly, the typical ISI, indexed by the peak time, aligns well with the duration of theta cycles observed in the primate visual system [12]. Similar theta-rhythmic active sensing occurs in various sensory systems of numerous species, including theta-rhythmic whisking or sniffing in rodents [13-15].

In primates, theta-rhythmic sampling has so far been primarily described in the context of distributed covert attention. For example, attentional benefits in processing a given stimulus (i.e., improved change detection accuracy) are modulated theta rhythmically and in anti-phase between two simultaneously monitored stimuli [8, 16-21]. These findings suggest theta-rhythmic shifts of covert attention, independent from large reorienting saccades. However, these findings have been vigorously debated [22, 23]. During fixation, covert shifts of attention might be reflected in the directions of small saccades [24], named micro-saccades, which have been directly linked to theta rhythms in the brain [12]. It has been suggested that micro- and macro-saccades are part of the same continuum of eye movements, differing only in scale [11, 25]. If both forms of saccades indeed operate under the same mechanistic framework, they might exhibit similar theta rhythmicity [26] While the subject of saccade rhythmicity has been explored, there is no consensus, and the prevailing notion leans toward an arrhythmic occurrence of saccades [27-29].

Here, we investigate saccade dynamics in two macaques and a cohort of 22 human participants under different spatial scenes, tasks, and conditions and quantify internally generated temporal patterns and saccade rhythmicity.

Methods

Participants and animals

Twenty-five adult human participants (12 male, 13 female) recruited from the public participated in the current study. We excluded three participants (all female) due to insufficient number of trials. All human participants had normal vision and provided informed consent. The study was approved by the local ethics committee.

Two adult rhesus macaques (*Macaque mulatta*, denoted C and G in the main text, both 19 years old) participated in this study. All experimental procedures were conducted in compliance with the German and European animal protection laws. The experiment was approved by the responsible local authority (Regierungspräsidium Darmstadt). Both animals were implanted with a titanium headpost [30]. Monkey G had a recording chamber implanted for addressing other scientific questions. To maintain motivation during the behavioral task, a small juice reward was given after each correct trial.

Tasks

An illustration of the task for both humans and macaques can be found in Supplementary Figure S1.

Macaque task

Macaques performed two tasks in separate sessions. Each session consisted of only one task. A specific set of conditions were included in each task and are listed below.

Task 1 consisted of both REGULAR and NOISE conditions. Each trial in both conditions began with the animal fixating at the center of the screen on a fixation dot (diameter 0.1 dva, i.e. degrees of visual angle). After fixation for 800 to 1000 ms, the fixation dot was turned off, followed by a ~100 ms gap. The search array was then presented. The array consisted of white filled dots (diameter 0.3 dva) that reflected potential saccade targets (see Supplementary Figure S1 for an illustration). Within the search array, 20% of the presented dots were real targets. The animal's task was to sequentially look at the dots to find any one of the real targets (foraging). During the foraging, if the animal's gaze landed inside a fixation window around a real target (radius 1.0 dva, not visible to the monkey), that target was replaced by an image of grapes, and a small juice reward was provided. If the monkey kept fixation on the grapes (harvesting), multiple pulses of reward were provided every 200 ms until a maximum harvesting window of 2000 ms had passed. Due to these rhythmic reward pulses, the data from the macaque post-search fixation was not used in the rhythmicity analyses. If the maximum search time passed (5000 ms) and none of the real targets had been foveated, the trial was terminated without a reward. In the REGULAR condition, the dots in the search array were spaced as if they were the centers of an invisible hexagonal tiling. In the NOISE condition, the search array contained the same number of dots as in a REGULAR trial, but the positions of the dots were randomly redistributed across the full screen to break any spatial regularity (Supplementary Figure S1).

Task 2 consisted of the IMAGE condition only, and also began with the animal fixating at the central fixation dot. This pre-search fixation for the IMAGE condition was identical to the REGULAR or NOISE conditions. After fixation for 800 to 1000 ms, the fixation dot was turned off, and after a ~100 ms gap, it was replaced by a natural image (16 * 21 dva, McGill Calibrated Colour Image Database, http://tabby.vision.mcgill.ca). From the moment the fixation dot was turned off, the animal was free to explore the image. After a random delay of 100 ms to 1900 ms, a small white dot (either 0.1 dva radius or 1.7 dva radius), the target, appeared at a random location within the image. We used two different radii for comparison that is not relevant to the current study. The monkey's task was to locate this target within a period of 5000 ms. If the target dot was found, the trial proceeded as described for Task 1.

Human tasks

Human participants performed two different tasks. In each session only one task was used. A specific set of conditions were included in each task that is listed below.

Task 1 consisted of REGULAR, NOISE, and IMAGE conditions. These conditions for human participants were identical to the respective conditions for macaques, except for the following differences: (1) The pre-search fixation duration was 2500 to 3500 ms; (2) the post-search fixation duration was also 2500 to 3500 ms and did not contain a repetitive reward, such that saccade rhythmicity could be analyzed during this period for human participants; (3) in all conditions, successful trial completion was indicated by a short audio feedback. If the maximum search time passed and no target was found, the trial was terminated.

Task 2 included REGULAR and IMAGE conditions. It was identical to Task 1, except for the following differences: (1) The REGULAR condition in Task 2 contained three different spacings of the grid (hexagon radius of 2.3, 4.5, and 8.5 dva); (2) the IMAGE condition remained unchanged from Task 1 despite a different set of images being used.

Data Analysis and Recording

All visual stimulation was controlled by custom software (https://github.com/esi-neuroscience/ARCADE) and presented on an LCD monitor. For monkeys, the monitor was an LG 32GK850G-B with a refresh rate of 143.9 Hz. For human participants, the monitor was a ViewPixx (VPixx Technologies Inc) with a refresh rate of 120 Hz. In both species, we recorded binocular gaze data

at 500 Hz using an EyeLink-1000 system (SR Research Ltd.). All gaze data were up-sampled to 1 kHz for further analyses. Real-time gaze data from the dominant eye was utilized for online behavioral control such as the pre- and post-search fixation periods.

The human data were collected across one or two sessions, with some participants attending only the first session and others participating in both. The first session used Task 1, the second Task 2. The first session included a brief training block to ensure participants gained experience with the online eye-tracking control and to fully understand the task. The experimental paradigm encompassed up to six blocks with the REGULAR, NOISE, and IMAGE conditions randomly interleaved. Each block consisted of 60 trials, 20 of each condition. Participants worked on one block until 60 correct trials (20 of each condition) were achieved. Participants were encouraged to complete all six blocks; however, the total number completed was contingent upon each participant's level of fatigue. The experimental design sought to prioritize participant comfort and data accuracy over the volume of completed blocks. The second session used the same approach, but for Task 2.

Saccade detection

We used a convolutional neural network for (micro)saccade detection [31]. We trained two separate networks for humans and macaques on randomly selected trials from each species. First, we labeled macro- and micro-saccades as separate classes in the data using a custom GUI (https://github.com/timnaher/IPyLabel). Next, we trained networks for humans and macaques separately. After epoching the data into trials, we replaced blinks with NaNs. Subsequently, we first detected (micro)saccades for each eye separately, and then accepted saccades only if they occurred in both eyes simultaneously. For all (micro)saccades, we enforced a minimum duration of 6 ms and a minimum separation between two subsequent events of 15 ms.

Rhythmicity index

We defined a rhythmicity index (RI) based on the coefficient of variation (CV) of the ISI distributions. As the ISI distributions show a log-normal form, we used the geometric CV (geoCV). The geoCV measures the dispersion of the ISI distribution in relation to its mean. We defined the RI as the inverse of the geoCV, such that higher RI values correspond to increased rhythmicity. Thus, RI is defined as:

$$RI = \frac{1}{geoCV}$$

, where geoCV is defined as:

$$geoCV = \sqrt{e^{s_{ln}^2} - 1}$$

, where s_{ln} is the ISI standard deviation of the ISI distribution after a natural log transformation. Using a CV-based measure to determine regularity has the advantage that it is scale-invariant and dimensionless, allowing to determine rhythmicity for many different processes. This property is important for our comparisons of slow versus fast saccades, because the RI can indicate preserved rhythmicity during both high and low saccade rates.

Expected RI for a Poisson process

To compute the expected RI for a Poisson process, we need to consider its inter-event-interval distribution, which is an exponential distribution. For a Poisson process with rate λ, the exponential distribution has mean $\mu = \frac{1}{\lambda}$ and standard deviation $\sigma = \frac{1}{\lambda}$. Since the CV is defined as $\frac{\sigma}{\mu}$, the expected RI of a Poisson inter-event-interval distribution is 1.

Statistical analyses

Throughout the study, we used paired and independent non-parametric tests such as the Wilcoxon rank sum test and the Wilcoxon signed rank test. Where appropriate, we corrected for multiple comparisons across conditions by using the Benjamini-Hochberg procedure with a family-wise error rate (FWER) of 0.05.

For the results presented in Figure 1, the statistical inference for the human-participant data was computed on a group level. This means we computed the average RI for each condition and each participant and then performed Wilcoxon signed rank tests between the conditions. Since the macaque sample consists of two animals, we used a within-subjects approach and tested for differences between conditions separately for each animal. Since the animals performed a different number of trials for each condition, we used an independent sample test, namely a Wilcoxon rank-sum test. To test whether humans and macaques showed RI values above the value expected for a Poisson process, i.e. above RI=1, we used a one-sample Wilcoxon signed rank tests where we subtracted 1 from the observed rhythmicity indices to reflect the differences from the expected RI value for a Poisson process.

To compare RIs between the three saccade-rate bins (Figure 2), we used Wilcoxon rank-sum tests. We computed these tests for both species separately. For the monkeys, we collapsed over individuals. The human participants were tested on a group level.

For the correlation analysis between saccade rate and RI, we used Spearman's rank correlation. We selected only trials which had 6 or more saccades and then computed the RI and saccade rate per trial. We report two separate analyses, one that pooled over participants and conditions, and a second one that computed the individual correlations per participant.

To compare the MACRO-MICRO rhythmicity to MACRO-MACRO and MICRO-MACRO rhythmicity, we used Wilcoxon rank-sum tests.

ISI peak difference analysis

To test for differences in ISI peaks, we fitted log-normal distributions to each participant's ISIs in the domain 0 to 1000 ms. We then took the peak of each fit as the peak ISI, or characteristic time.

Poincaré plots and analyses

To analyze the ISI time-series data in the Poincaré space, we first created scatter plots, where each dot corresponds to a pair of two subsequent ISIs (ISI_n and ISI_{n+1}), with the dot's x-value corresponding to the ISI_n and the y-value corresponding to the ISI_{n+1} (see Figure 5B for an example). In Poincaré space, the y-values in a given x-axis bin constitute the probability mass function of all ISI_{n+1} that follow a given ISI_n value. If ISIs were statistically independent, these probability mass functions would not depend on ISI_n, and would therefore be equal. To assess this, we can compare the central moments of these probability mass functions to see if they change systematically, thereby revealing a correlation structure. Like Rodieck, et al. [32], we focused on the first central moment, the mean. We separately investigate the means of all y-values in a given x-axis bin, and the means of all x-values in a given y-axis bin. Note that the mean of all y-values in a given x-axis bin corresponds to the weighted sum of the histogram of the y-values in this x-axis bin [32], and vice versa: The total number of data points was

determined by summing all the frequencies; The mean of the histogram data was then derived by dividing the weighted sum by the total frequency [32]; In cases where the total frequency was zero, indicating an absence of data points, the mean was designated as NaN.

Windowed RI

In the last analysis (Figure 5), we computed RI values for sliding windows of 11 ISIs for the movie free-viewing condition. It is important to highlight that we shifted the window by only one sample at a time, resulting in overlapping windows. We only considered complete windows, i.e. we discarded the first and last 10 samples of the ISI time-series.

Results

Saccade rhythmicity is influenced by spatial structure

Numerous studies have revealed that saccadic eye movements display a characteristic unimodal inter-saccadic interval (ISI) distribution, marked by a pronounced rightward skew. This unimodal distribution is well described by a log-normal shape, effectively representing both the unimodality and the pronounced rightward skew (Figure 1A-B,D-E). ISI distributions are a type of inter-event-interval distribution, which are widely used in the analysis of rhythmic neuronal spiking activity, and other point-process time series. They can provide valuable insights into the temporal dynamics of the process that generated the events. This makes ISI distributions an effective tool for gaining insights into the temporal dynamics of saccades as well. Therefore, we analyzed the ISI distributions across different conditions of our task, testing for potential variations and patterns.

We investigated whether spatial structure in the visual input has an influence on the saccade rhythmicity in humans and macaque monkeys. To test this, we designed a visual search task, where subjects were instructed to find a hidden reward by saccading to possible target points on the screen. These target points were presented as either a regular hexagonal grid (REGULAR condition) or a shuffled grid without spatial regularity (NOISE condition). Additionally, we used a condition, in which a target appeared at a random time and location on a natural image, and participants saccaded to it (IMAGE condition; see Methods for details). These different conditions showed high spatial periodicity in the REGULAR condition and low spatial periodicities for the other two conditions.

We present an analysis of saccade rhythmicity in relation to the spatial periodicity of the visual input during the search task. For this analysis, we defined a rhythmicity index, RI=1/CV, with CV being the geometric coefficient of variation of the ISI distribution (see Methods). The RI value increases when the corresponding inter-event-interval distribution becomes narrower, which reflects that the underlying process becomes more regular in time. The RI for a Poisson process is always one, irrespective of its rate (this is because the inter-event-interval distribution of a Poisson process is exponential, see Methods for details). Our findings indicate a clear dependence of the RI on the visual input conditions, with similar patterns for both species (Figure 1 C,F).

In human participants, intriguingly, the NOISE condition displayed the highest RI (mean RI = 2.69), followed by the REGULAR condition (mean RI = 2.51), while the IMAGE condition showed the least rhythmicity (mean RI = 2.11). The differences between all pairs of the three conditions were significant (REGULAR vs. NOISE, W = 44.00, $p = 2.21 \times 10^{-2}$; NOISE vs. IMAGE, W = 8.00, $p = 3.59 \times 10^{-4}$; REGULAR vs. IMAGE, W = 31.00, $p = 5.80 \times 10^{-3}$). Among the human ISI distributions, the REGULAR and NOISE conditions exhibited only minimal differences, whereas the IMAGE condition revealed a shifted ISI peak along with a heavier tail (Figure 1A) consistent with the lower RI. These analyses were based on group-level statistics.

In macaques, the ISI distributions appeared quite similar to the humans, with almost indistinguishable REGULAR and NOISE conditions, and a heavier tail for the IMAGE condition, albeit less pronounced compared to humans. To analyze the differences in RI, we utilized within-subject tests separately for both monkeys, calculating the RI for each trial instead of aggregating all trials per condition. Monkey G (Figure 1F, lower line) displays a pattern similar to that of humans, with the NOISE condition showing the highest RI, followed by the REGULAR and IMAGE conditions (regular vs. noise, W = 86203, $p = 1.20 \times 10^{-3}$; regular vs. image, W = 315142, $p = 5.38 \times 10^{-2}$; noise vs. image, W = 353983.0, $p = 2.48 \quad 10\text{-}^{12}$). However, the difference between REGULAR and IMAGE is not significant after correction for multiple comparisons (p = 0.53). Conversely, Monkey C (Figure 1F, upper line) demonstrates a slightly different pattern, where the REGULAR condition exhibits the highest rhythmicity, followed by the NOISE and IMAGE conditions (REGULAR vs. NOISE, W = 329,826.0, $p = 4.37 \times 10^{-2}$; REGULAR vs. IMAGE, W = 434,799.0, $p = 5.76 \times 10^{-65}$; NOISE vs. IMAGE, W = 169,895.0, $p = 2.99 \times 10^{-32}$).

For all tested conditions, the observed RIs surpassed the RI value of one that is expected for a Poisson process (humans: REGULAR, NOISE, IMAGE: W = 0, $p = 4.0 \times 10^{-5}$, monkey C: REGULAR: W = 4, $p = 2.54 \times 10^{-227}$, NOISE: W = 1, $p = 2.03 \times 10^{-85}$, IMAGE: W = 0, $p = 5.20 \times 10^{-174}$; monkey G: REGULAR: W = 2, $p = 2.53 \times 10^{-65}$, NOISE:W = 0, $p = 2.02 \times 10^{-85}$, IMAGE:W = 0, $p = 2.49 \times 10^{-286}$). This suggests that the saccade dynamics under all tested conditions reflect a more organized temporal structure than expected if saccades were generated according to a Poisson process.

Fast saccades are more rhythmic

So far, we evaluated saccade rhythmicity based on an analysis of the features of the ISI distributions under different conditions. A parallel method to examine temporal statistical dependencies within a time series is by assessing its autocorrelation function (ACF). The ACF gauges the correlation of a time series with a lagged version of itself, allowing the identification of recurring patterns. Previous research has indicated the ACF of saccades for human participants to be highly variable [33]. Given the characteristic heavy-tail shape of the ISIs, it is conceivable that faster saccades might be more rhythmic. To test this, we derived the saccade rate per trial and sorted trials into three bins of equal trial numbers. Trials with the highest saccade rates exhibited the most structured ACF for both species: humans show two side peaks and macaques four. Conversely, trials with the lowest saccade rates barely show one side peak for humans, and merely two for macaques (Figure 2 A,D). A comparison of the separate autocorrelation functions per saccade rate bin (Figure 2 A,D) with the autocorrelation functions pooled over saccade rates (Supplementary Figure S2,B,C) suggests that a pooled approach underestimates saccade rhythmicity.

As anticipated, sorting the trials into different saccade-rate bins resulted in a shift in the peak of the ISI distribution for each bin (Figure 2, C,F), with humans showing longer ISIs (low: 260 ms, medium: 235 ms, high: 210 ms) than macaques (low: 220 ms, medium: 209 ms, high: 198 ms). We observed that decreasing saccade rates were associated with increasing standard deviations (SDs) of ISIs (humans: 116.6, 137.0, 188.2; macaques: 76.9, 84.0, 97.6, for high, medium, low saccade rates, respectively). In fact, the SDs of the ISIs increased over-proportionally compared to the peak times of the ISIs. Correspondingly, trials with low saccade rates showed reduced RIs: RIs were lower for low than medium saccade rate (W = -3.82, $p = 1.95 \times 10^{-4}$), for medium than high rate (W = -2.37, $p = 1.77 \times 10^{-2}$), and for low than high rate (W = -4.90, $p = 2.79 \times 10^{-6}$) in humans on a group level. Similarly, pooling both macaques, compared on a trial level, RIs were lower for low than medium rate (W = -8.46, $p = 3.75 \times 10^{-17}$), medium than high rate (W = -7.48, $p = 6.93 \times 10^{-14}$), and low than high rate (W = -14.93, $p = 5.78 \times 10^{-50}$). Note that the RI is normalized for saccade rate, such that higher saccade rates do not trivially lead to higher RI. Note further that also generally, a point process with a higher rate is not necessarily more rhythmic.

Besides binning the data into low, medium, and high saccade rate bins, we also calculated the rank correlations between saccade rate and RI, across trials. When pooling over all human participants, we obtained a positive correlation between saccade rate and RI ($\rho = 0.275$, $p = 2.53 \times 10^{-6}$, the distribution of individual correlation coefficients can be found in Supplementary Figure S2A). When repeating the same analysis for the macaques, we also found a positive correlation in the pooled data ($\rho = 0.229$, $p = 3.21 \times 10^{-16}$). However, when inspecting the individual macaques, we observe that only monkey C shows a positive correlation ($\rho = 0.333$, $p = 6.46 \times 10^{-64}$) and monkey G shows a negative correlation ($\rho = -0.206$, $p = 4.16 \times 10^{-19}$). These analyses reveal that trials with high saccade rates typically exhibit substantial saccade rhythmicity (Figure 2 B,E).

Fixational eye movements are affected by the visual scene

In all three conditions (REGULAR, NOISE, IMAGE), each trial began with the pre-search fixation of a white dot on a gray screen (see Methods). This initial fixation then gave way to the search task, the results of which are presented in Figure 1. For humans, once they had located the target, they were requested to maintain fixation on it for a post-search fixation between 2.5 and 3.5 seconds. It was only after this successful fixation that the reward sound was played, and the trial concluded. During the post-search fixation, the search display remained on the screen, and differences to the pre-search period might be due to this difference in visual stimulation or the preceding search period. We investigated micro-saccades during the pre- and post-search periods and compared them to saccades during the search period.

Figure 3 shows the ISI distributions for pre-search, search, and post-search (micro-)saccades including log-normal fits. It is evident that in all three conditions and for both species, ISI distributions were unimodal, suggesting the presence of a characteristic time (ISI peak) of (micro-)saccades during search and fixation periods.

To compare the conditions at the three task positions, we performed selected Wilcoxon-tests. During the pre-search, the conditions were not different, as was to be expected, because at this time the task did not differ between conditions. In the search period, the peak times for the REGULAR and NOISE conditions were not different, whereas for the IMAGE condition, they were slower than both other conditions (REGULAR vs IMAGE: $W = 2$, $p = 4.23 \times 10^{-4}$; NOISE vs IMAGE: $W = 0$, $p = 3.58 \times 10^{-4}$). Interestingly, the ISI distributions during the post-search period displayed a pattern similar to the search period (REGUAR vs IMAGE: $W = 28$, $p = 9.15 \times 10^{-3}$, NOISE vs IMAGE: $W = 27.5$, $p = 9.15 \times 10^{-3}$). These differences in the post-search period cannot be attributed to the task demand, which is identical (fixation), but need to be attributed to the surrounding visual stimulation or the preceding search period.

Micro-saccade rhythmicity reflects fixation specificity

After exploring the dynamics of micro-saccades during the pre- and post-search fixation intervals, we will investigate their natural occurrence during one of our task conditions. Based on previous work, we hypothesized that micro-saccades would occur during free viewing of the REGULAR condition, particularly when the grid spacing exceeded a certain threshold [34]. We presented seven human participants with three distinct spacing conditions: SMALL, MEDIUM, and LARGE, representing grid spacings of 1.3 dva, 2.3 dva, and 4.9 dva, respectively. Saccade metrics like amplitude and peak velocity showed similar distributions for the SMALL and MEDIUM conditions, yet showed different, bimodal, distributions in the LARGE condition (Supplementary Figure S3A). Correspondingly, the scatter plot of peak velocity versus amplitude, i.e., the main sequence plot, shows two clearly separate clusters of saccades (Supplementary Figure S3B).

The emergence of these clusters in the LARGE condition can be attributed to frequent naturally occurring micro-saccades during the visual search. When target spacing exceeded a certain threshold, macro-saccades tended to undershoot targets, and were followed by corrective secondary micro-saccades that bridged the remaining distance, in agreement with previous research [35, 36]. An example eye-position trace from the LARGE condition illustrates that a macro-saccade (blue trace) was regularly followed by a micro-saccade (purple trace) (Figure 4A). Correspondingly, a sequence of saccade amplitudes, from another example trial, shows the tendency of alternation between macro- and micro-saccades (Figure 4B). Average transition probabilities (over trials and human participants) revealed that macro-saccades were followed in 72% by micro-saccades and in only 28% by another macro-saccade; conversely, micro-saccades were followed in 93% by macro-saccades, and in only 7% by another micro-saccade (Figure 4C). These corrective micro-saccades exhibited a strong directional bias, aligning with the preceding macro-saccade. When the directions of corrective micro-saccades are expressed relative to the direction of the preceding macro-saccade, the distribution of directional differences is highly non-uniform and unimodal with a mean close to zero (Rayleigh test for uniformity, $p = 3.31 \times 10^{-53}$, Figure 4E, illustrated in Figure 4D).

This phenomenon of secondary corrective micro-saccades has been documented before in controlled, single-saccade tasks. Our results highlight the natural occurrence of the phenomenon in a free-viewing task setting. After delineating the spatial characteristics of these corrective micro-saccades, we turned our attention to their temporal dynamics by examining the ISI distributions for MACRO-TO-MACRO, MICRO-TO-MACRO, and MACRO-TO-MACRO sequences (Figure 4F). It is apparent that all ISI distributions embody the typical log-normal shape, yet also show distinct differences. Notably, the MACRO-TO-MICRO ISI distribution revealed a smaller tail in comparison to the other distributions. This might reflect the reduced planning requirements preceding corrective micro-saccades. This is also reflected in an increased RI at the MACRO-TO-MICRO condition compared to MACRO-TO-MACRO ($W = 2.49$, $p = 1.90 \times 10^{-2}$) and MICRO-TO-MACRO ($W = 3.13$, $p = 5.23 \times 10^{-3}$). Nevertheless, the peak of the MACRO-TO-MICRO ISI distribution is still within 20 ms of the other ISI distribution peaks, indicating the existence and, most importantly, the stability of the characteristic timing of saccades. The MICRO-TO-MACRO saccade ISI distribution again presents the typical heavy tail, appearing visually identical to the MACRO-TO-MACRO ISI distribution. This aligns with the notion that the period between these saccades is a standard task-related fixation wherein the visual system plans the following macro-saccade. These findings underscore that the dynamics of regularity are influenced by the specific task the visual system performs during each fixation.

Subsequent ISIs are not independent

So far, we based the rhythmicity analysis on a global RI which was calculated for the time-collapsed ISI data. Although this index provides a summary measure of the rhythmicity of a process, it neglects the ISI sequence. To further analyze the sequence of ISIs, we investigated saccades during a free-viewing movie session. Here, participants watched naturalistic movies and were free to explore the movie scenes without any task requirements. We analyzed the ISI dependencies in this free-viewing setting, to detect any temporal correlations. We found a strong positive autocorrelation for ISIs up to a lag of 20 (Figure 5A). To further analyze the sequence of ISIs, we created scatter plots, where each dot corresponds to a pair of two subsequent ISIs (ISI_n and ISI_{n+1}), with the dot's x-value corresponding to the ISI_n and the y-value corresponding to the ISI_{n+1} (see Figure 5B for an example). This type of self-embedding is referred to as Poincaré plot, and it allows an analysis of a space, which reflects the temporal dynamics and correlation structure of the time series.

In this Poincaré space, the y-values in a given x-axis bin constitute the probability mass function of all ISIn+1 that follow a given ISIn value. If ISIs were statistically independent, these probability mass functions would not depend on ISIn, and would therefore be equal. To assess this, we can compare the

central moments of these probability mass functions to see if they change systematically, thereby revealing a correlation structure. Similar to Rodieck, et al. [32], we focused on the first central moment, the mean (after normalization as detailed in Methods). We plot (grey dots in Figure 5C) the means of all y-values in a given x-axis bin. If these means do not fall on a straight line parallel to the x-axis, this is an indication for a dependence of subsequent ISIs. The corresponding analysis can also be performed for the x-values in each y-axis bin (black dots in Figure 5C). The resulting point clouds indeed do not fall on a straight line parallel to the respective axes, but rather seem to follow a semi-logarithmic function, suggesting that the inter-dependency is higher for shorter ISIs. Similar observations were made for the REGULAR, NOISE and IMAGE conditions (Supplementary Figure S4). This finding aligns with the observation that trials with higher saccade rates show ISIs that are more rhythmic (see Figure 2A,B,D,E).

A closer examination of the ISI time series revealed epochs of low variability in subsequent ISIs, corresponding to high rhythmicity (orange epoch in Figure 5B,D,E). These epochs were interspersed with epochs of variable ISIs, corresponding to low rhythmicity (green epoch in Figure 5B,D,E). Our findings indicate that, in the absence of task constraints, the visual system fluctuates between shorter, more rhythmic ISIs, and longer, less rhythmic ISIs. While long ISIs could in principle also occur rhythmically, our data did not provide evidence for this. Instead, when moving windows of 11 consecutive ISIs were used to calculate local ISI mean and RI, there was a clear negative correlation between the ISI mean and the RI (mean r = -0.440, SE = 0.048; N = 14 participants).

In summary, these results suggest a scale-dependency in the dispersion of the ISI distribution, and therefore, in saccade rhythmicity. They also suggest a dynamism in the visual system, characterized by an alternation between states of fast saccades with high rhythmicity and slow saccades with decreased rhythmicity.

Discussion

We explored the temporal dynamics of human and macaque saccades during a variety of different visual stimulation and task conditions. We show that saccade rhythmicity is not merely a byproduct of spatial regularity of the visual scene, and that saccades exhibit temporal regularity well above a Poisson process. Both micro- and macro-saccades show similar characteristic inter-saccadic intervals, further supporting the hypothesis that they are manifestations of the same process, differing only in scale. These characteristic intervals can undergo slight shifts depending on the visual scene and the task at hand. When natural exploration entails corrective micro-saccades, their ISI distribution is particularly narrow, suggesting reduced variance in saccade generation during this likely automatized process. Lastly, in a naturalistic free-viewing paradigm, the visual system fluctuates between states of high and low rhythmicity, with states of high rhythmicity corresponding to periods of high saccade rate.

The brain's sampling of the visual environment exhibits a characteristic temporal pattern, as evidenced by the peaked ISI distributions. Yet, the temporal dynamics of saccades do not follow a strictly periodic regime [33]. Based on these observations, we propose a conceptual model that reconciles the temporal dynamics of saccades with the existing knowledge of theta rhythmic sampling in active sensing. Specifically, we propose that the interval between two consecutive saccades consists of two primary components: a relatively consistent, regular component and an additive, more variable component. This aligns with a generative mechanism that adds two processes: A fundamentally periodic process, albeit with noise, some cycle-length variability, and some optional cycle skipping, together with an additive, non-periodic component. The periodic process might be anchored in the theta-generating mechanisms observed in primate attentional sampling and non-primate active sensing, suggesting a foundationally rhythmic sampling routine.

Note that a periodic process that triggers a saccade at a specific phase and is then phase-reset by the saccade is essentially equivalent to a rise-to-threshold process that triggers a saccade at a specific threshold and is then reset by the saccade [37]. Such diffusion processes have been used to describe saccadic reaction times, primarily in tasks with an extrinsic structure, such as the onset of a saccade target [37-39]. Both, periodic and diffusion processes implement a rise to threshold and a reset and are therefore conceptually similar to the suggestion that saccade generation is a self-paced process [33]. If the slope of this rise decreases, the resulting inter-reset interval distribution becomes wider and its peak shifts to longer intervals. This is what we observed when comparing the REGULAR and NOISE conditions to the IMAGE condition. Yet, when we compared the ISI distributions of MACRO-TO-MACRO sequences with MACRO-TO-MICRO sequences, we found that the distributions become substantially narrower, while their peaks remained nearly identical. This latter observation is hard to explain by merely changing the slope of a rise-to-threshold model; it is easy to explain when we postulate that there is additive noise in the diffusion strength, i.e., in the momentary slope.

The relatively consistent, regular componen11t potentially mirrors the standard duration required by the visual system to execute fundamental visual processing routines, such as a single feed-forward sweep, and possibly a feedback sweep [40]. We consider the finding that in both, humans and macaques, micro- and macro-saccades exhibit a similar peak in their ISI distributions as an indicator for the existence and inter-species stability of this characteristic sampling time in primates. Nevertheless, there can still be slight shifts in this characteristic time when the visual scene becomes more complex and therefore likely more difficult to process (Figure 3, larger peak times in the IMAGE condition). Yet, when the task the visual system has to solve at a fixation is straightforward, the system can rely on this inherent timing, prompting the subsequent saccade within the typical ISI duration. An example for this can be found in this study, when the visual system generates corrective micro-saccades during the LARGE spacing condition (Figure 4). Note that in this case, the visual system produces inter-saccadic intervals that are particularly close to the typical inter-saccadic intervals; it does not produce intervals that are close to the minimal observed ISI, which might be taken as an estimate of the physiologically possible minimal ISI.

A rhythmic visual sampling routine might have been favored during evolution for at least two purposes: (1) providing an optimal time frame for processing new visual inputs and (2) ensuring that rhythmic excitability fluctuations within the visual system are temporally synchronized to best process post-saccadic inputs. In this framework, saccades are both influenced by the ongoing oscillation and play a role in its partial reset. This quasi-rhythmic routine is then complemented by an additive, cognitive component to cater to specific processing demands. This proposed mechanism is tailored for active sensing, encompassing the entire spectrum from sensory input to motor output, and the coordination across these stages.

The variable strength of the additive component was particularly evident in our analysis of the free exploration of natural movies. This analysis revealed that epochs of lower rhythmicity, i.e., with higher additive component, are interleaved with epochs of higher rhythmicity, i.e. with lower additive component. Intriguingly, epochs of high rhythmicity contained ISIs that tended to be close to the characteristic ISI, and thereby relatively short. This meta-dynamic of saccade rhythmicity was revealed by using Poincaré plots and analyzing rhythmicity in a time-varying manner, i.e., in sliding windows. These approaches revealed that the observed positive ISI autocorrelation is present specifically between short-ISI saccades. Crucially, these approaches avoided a global pooling of ISIs, which would have failed to reveal the large degree of rhythmicity that the system can show at times.

When interpreting the pronounced tail in the ISI distributions as a manifestation of an additive and possibly cognitive component, the macaque data offers an intriguing perspective. The more

pronounced rhythmicity observed in macaques, characterized by a less extensive tail but a comparable characteristic time, might be attributed to a relatively diminished cognitive component, compared to humans, influencing the variability at each fixation. However, an alternative explanation could be their extensive training in saccadic tasks, which might lead to more automatized and stereotypical saccade behavior. Along a similar line, rodent active sensing during whisking and sniffing might be even more rhythmic than primate active sensing by saccades. This might be due to reduced cognitive components in rodents. Yet, it might also reflect a larger complexity (and heterogeneity thereof) across visual samples as compared to olfactory or tactile samples. This increased complexity in visual samples might demand multiple processing sweeps, requiring flexibility in processing time at each fixation. In this case, a rigidly periodic sampling regime might be disadvantageous.

To further test the hypothesis that saccades might be fundamentally driven by an inherent, theta-like process with additive noise, it will be a fruitful task for future studies to investigate neuronal correlates of such a process. Additionally, to test the hypothesis of additive cognitive noise, one could modulate brain areas associated with saccadic sampling such as FEF, LIP and V1. Future studies could focus on systematically varying task demands, overall perceptual goals, and modulating brain activity to reveal the mechanisms underlying the temporal structure of saccadic eye movements.

Acknowledgements

The authors would like to thank Ece Nur Uygur for help with the human data acquisition and Lisa Bastian for helpful discussions on the manuscript. This work was supported by DFG (FOR 1847 FR2557/2-1, FR2557/7-1).

Author contributions:

T.N.: Conceptualization, Data curation, Formal analysis, Investigation, Methodology, Resources, Software, Visualization, Writing – original draft, Writing, review & editing. Y.Z.: Conceptualization, Formal analysis, Data curation, Investigation, Methodology, Resources, Software, Visualization, Writing – original draft, Writing, review & editing. M.P.: Investigation, Writing, review & editing. P.F.: Conceptualization, Supervision, Writing – original draft, Writing, review & editing.

Declaration of interests

P.F. has a patent on thin-film electrodes and is member of the Advisory Board of CorTec GmbH (Freiburg, Germany). The authors declare no further competing interests.

Figure legends

Figure 1: A Human ISI distribution for REGULAR, NOISE, and IMAGE**. B** Human cumulative ISI distributions, for the three conditions. **C** Rhythmicity indices, defined as 1/geoCV, for the three conditions. Horizontal dashed line indicates the rhythmicity index of a Poisson process. **D-F**, same as A-C, but for macaques. *$p < 0.05$, **$p < 0.01$, *** $p < 0.001$

Figure 2: A Autocorrelation functions of macaque saccades for trials with high saccade rate (purple), medium saccade rate (orange) and low-saccade rate (green). Autocorrelations were smoothed with a 50 ms boxcar. **B** Rhythmicity index for the three saccade-rate bins. Significance stars are based on Wilcoxon rank-sum tests with Benjamini-Hochberg correction for multiple comparisons (FWER = 0.05) **C** ISI distributions for the three different saccade-rate bins. **D-F**, same as **A-C**, but for humans. Human participants were tested on a group level. *$p < 0.05$, **$p < 0.01$, ***$p < 0.001$

Figure 3: A Pre-search, search, and post-search ISI distributions for humans. The solid line shows a log-normal fit, the peak of the fit is indicated by the vertical dashed line. Peak time can be found in the upper right corner of each subpanel. **B** Same as **A** but for the macaques. The post-trial fixation data in macaques were excluded (see Methods). **C** Comparison of peak times for the human data. For each participant, we fitted log-normal distributions to the ISI data and located the peaks. We determined significance using Wilcoxon tests and a Benjamini-Hochberg correction for multiple comparisons. **D** Same as **C**, but for the rhythmicity index. * $p < 0.05$, ** $p < 0.01$, *** $p < 0.001$

Figure 4: A Example trial of a human participant during the large-spaced REGULAR condition. The blue trace shows macro-saccades, the purple trace shows interleaved micro-saccades, and the gray disks show approximate fixation positions. **B** Example sequence of saccade amplitudes from a single trial. Saccade amplitudes tend to alternate between macro- and micro-saccades. **C** Transition probabilities between macro and micro saccades, averaged over trials and human participants. **D** Schematic representation of the observed naturally occurring sequence of macro-saccades and micro-saccades. **E** Distribution of differences of directions between micro-saccades and preceding macro-saccades. **F** ISI distributions for different sequences of macro- and micro-saccades, and the corresponding log-normal fits. Each sub-panel contains the peak location in ms and the rhythmicity index of the ISI distribution.

Figure 5: **A** Autocorrelation function of the free-viewing ISIs, averaged over all human participants. The shaded area represented ±1 SD. **B** Poincaré plot of one participant during free-viewing, including two example trajectories. The orange trace shows an example period of highly rhythmic ISIs. The green trace shows an example of a less rhythmic period. **C** Analysis of dependency of subsequent ISIs for the movie free-viewing condition, pooled over all participants. For the gray dots, the x-value of each dot corresponds to a millisecond bin on the x-axis, and the y-value corresponds to the mean of the respective bin's y-values (after normalization as described in Methods). For the black dots, the same holds, only switching axes. **D** Example ISI sequence from the same participant as in **B**. Traces from panel **B** are marked in orange and green. **E** Windowed (window size 11 ISIs) rhythmicity index (purple) and ISI mean (pink) for the example time series in **D**.

Supplementary Figure S1: Example of the task progression in the NOISE condition.

Supplementary Figure S2: A Spearman rank correlation coefficient between saccade rate and RI for individual participants. All human participants except 2 reached statistical significance at $p < 0.05$. **B** Autocorrelation function for all trials and all conditions in human participants. **C** same as **B** but for macaques.

Supplementary Figure S3: **A** Velocity (left) and amplitude distributions for the small (purple), medium (pink), and large (green) spacing conditions. **B** Saccade main sequence plot for small, medium, and large spacing. The vertical dashed lines reflect the distance between dots on the grid in dva.

Supplementary Figure S4: Poincaré analysis of dependency for subsequent ISIs for humans and macaques and different conditions.

References

1. Gibson, J.J. (1979). The ecological approach to visual perception, (Boston: Houghton Mifflin).
2. Zweifel, N.O., and Hartmann, M.J.Z. (2020). Defining "active sensing" through an analysis of sensing energetics: homeoactive and alloactive sensing. J Neurophysiol *124*, 40-48.
3. Findlay, J.M., and Gilchrist, I.D. (2003). Active vision : the psychology of looking and seeing, (Oxford ; New York: Oxford University Press).
4. Liversedge, S.P., Gilchrist, I.D., and Everling, S. (2011). The Oxford handbook of eye movements, (Oxford ; New York: Oxford University Press).
5. Lu, Y., Yin, J., Chen, Z., Gong, H., Liu, Y., Qian, L., Li, X., Liu, R., Andolina, I.M., and Wang, W. (2018). Revealing Detail along the Visual Hierarchy: Neural Clustering Preserves Acuity from V1 to V4. Neuron *98*, 417-428 e413.
6. Petras, K., Ten Oever, S., Jacobs, C., and Goffaux, V. (2019). Coarse-to-fine information integration in human vision. Neuroimage *186*, 103-112.
7. Desimone, R., and Duncan, J. (1995). Neural mechanisms of selective visual attention. Annu Rev Neurosci *18*, 193-222.
8. Fries, P. (2023). Rhythmic attentional scanning. Neuron *111*, 954-970.
9. Gilchrist, I.D., Brown, V., and Findlay, J.M. (1997). Saccades without eye movements. Nature *390*, 130-131.
10. Henderson, J.M. (2003). Human gaze control during real-world scene perception. Trends Cogn Sci *7*, 498-504.
11. Otero-Millan, J., Troncoso, X.G., Macknik, S.L., Serrano-Pedraza, I., and Martinez-Conde, S. (2008). Saccades and microsaccades during visual fixation, exploration, and search: foundations for a common saccadic generator. J Vis *8*, 21 21-18.
12. Spyropoulos, G., Bosman, C.A., and Fries, P. (2018). A theta rhythm in macaque visual cortex and its attentional modulation. Proc Natl Acad Sci U S A.
13. Ranade, S., Hangya, B., and Kepecs, A. (2013). Multiple modes of phase locking between sniffing and whisking during active exploration. J Neurosci *33*, 8250-8256.
14. Moore, J.D., Deschenes, M., Furuta, T., Huber, D., Smear, M.C., Demers, M., and Kleinfeld, D. (2013). Hierarchy of orofacial rhythms revealed through whisking and breathing. Nature *497*, 205-210.
15. Kepecs, A., Uchida, N., and Mainen, Z.F. (2007). Rapid and precise control of sniffing during olfactory discrimination in rats. J Neurophysiol *98*, 205-213.
16. Fiebelkorn, I.C., Saalmann, Y.B., and Kastner, S. (2013). Rhythmic sampling within and between objects despite sustained attention at a cued location. Curr Biol.
17. Helfrich, R.F., Fiebelkorn, I.C., Szczepanski, S.M., Lin, J.J., Parvizi, J., Knight, R.T., and Kastner, S. (2018). Neural Mechanisms of Sustained Attention Are Rhythmic. Neuron *99*, 854-865 e855.
18. Landau, A.N., and Fries, P. (2012). Attention samples stimuli rhythmically. Curr Biol *22*, 1000-1004.
19. Landau, A.N., Schreyer, H.M., van Pelt, S., and Fries, P. (2015). Distributed Attention Is Implemented through Theta-Rhythmic Gamma Modulation. Curr Biol *25*, 2332-2337.
20. Fiebelkorn, I.C., and Kastner, S. (2019). A Rhythmic Theory of Attention. Trends Cogn Sci *23*, 87-101.
21. van der Werf, O.J., Schuhmann, T., de Graaf, T., Ten Oever, S., and Sack, A.T. (2023). Investigating the role of task relevance during rhythmic sampling of spatial locations. Sci Rep *13*, 12707.
22. van der Werf, O.J., Ten Oever, S., Schuhmann, T., and Sack, A.T. (2022). No evidence of rhythmic visuospatial attention at cued locations in a spatial cuing paradigm, regardless of their behavioural relevance. Eur J Neurosci *55*, 3100-3116.
23. Brookshire, G. (2022). Putative rhythms in attentional switching can be explained by aperiodic temporal structure. Nat Hum Behav *6*, 1280-1291.

24. van Ede, F. (2023). Do microsaccades track shifting but not sustaining covert attention? Proc Natl Acad Sci U S A *120*, e2309431120.
25. Martinez-Conde, S., Otero-Millan, J., and Macknik, S.L. (2013). The impact of microsaccades on vision: towards a unified theory of saccadic function. Nat Rev Neurosci *14*, 83-96.
26. Hogendoorn, H. (2016). Voluntary Saccadic Eye Movements Ride the Attentional Rhythm. J Cogn Neurosci *28*, 1625-1635.
27. Wang, H.X., Freeman, J., Merriam, E.P., Hasson, U., and Heeger, D.J. (2012). Temporal eye movement strategies during naturalistic viewing. J Vis *12*, 16.
28. Leopold, D.A., and Logothetis, N.K. (1999). Multistable phenomena: changing views in perception. Trends Cogn Sci *3*, 254-264.
29. Harris, C.M., Hainline, L., Abramov, I., Lemerise, E., and Camenzuli, C. (1988). The distribution of fixation durations in infants and naive adults. Vision Res *28*, 419-432.
30. Psarou, E., Vezoli, J., Scholvinck, M.L., Ferracci, P.A., Zhang, Y., Grothe, I., Roese, R., and Fries, P. (2023). Modular, cement-free, customized headpost and connector-chamber implants for macaques. J Neurosci Methods *393*, 109899.
31. Bellet, M.E., Bellet, J., Nienborg, H., Hafed, Z.M., and Berens, P. (2019). Human-level saccade detection performance using deep neural networks. J Neurophysiol *121*, 646-661.
32. Rodieck, R.W., Kiang, N.Y., and Gerstein, G.L. (1962). Some quantitative methods for the study of spontaneous activity of single neurons. Biophys J *2*, 351-368.
33. Amit, R., Abeles, D., Bar-Gad, I., and Yuval-Greenberg, S. (2017). Temporal dynamics of saccades explained by a self-paced process. Sci Rep *7*, 886.
34. Frost, D., and Poppel, E. (1976). Different programming modes of human saccadic eye movements as a function of stimulus eccentricity: indications of a functional subdivision of the visual field. Biol Cybern *23*, 39-48.
35. Lisi, M., Solomon, J.A., and Morgan, M.J. (2019). Gain control of saccadic eye movements is probabilistic. Proc Natl Acad Sci U S A *116*, 16137-16142.
36. Hallett, P.E. (1978). Primary and secondary saccades to goals defined by instructions. Vision Res *18*, 1279-1296.
37. Ratcliff, R., and McKoon, G. (2008). The diffusion decision model: theory and data for two-choice decision tasks. Neural Comput *20*, 873-922.
38. Carpenter, R.H., and Williams, M.L. (1995). Neural computation of log likelihood in control of saccadic eye movements. Nature *377*, 59-62.
39. Trappenberg, T.P., Dorris, M.C., Munoz, D.P., and Klein, R.M. (2001). A model of saccade initiation based on the competitive integration of exogenous and endogenous signals in the superior colliculus. J Cogn Neurosci *13*, 256-271.
40. Lamme, V.A., and Roelfsema, P.R. (2000). The distinct modes of vision offered by feedforward and recurrent processing. Trends in neurosciences *23*, 571-579.

Figure 1

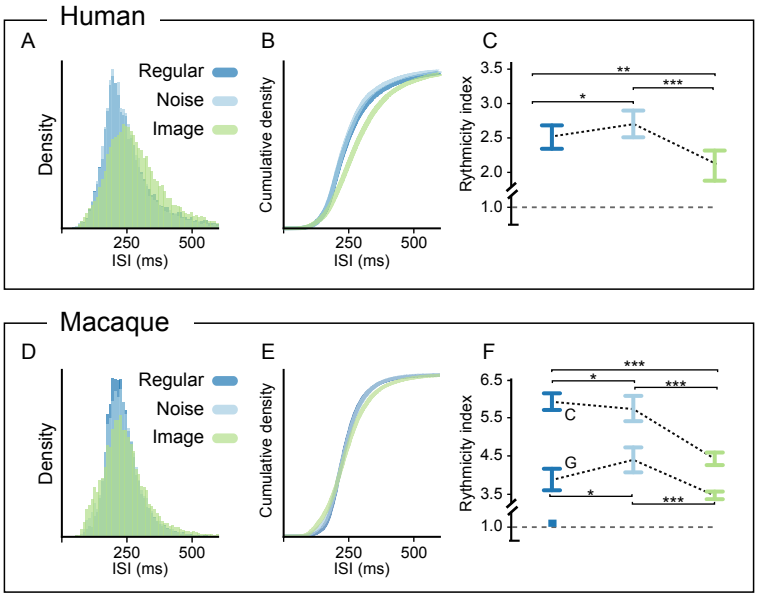
Human
A
Regular
Noise
Image
Density
250
500
ISI (ms)
B
Cumulative density
250
500
ISI (ms)
C
Rythmicity index
3.5
3.0
2.5
2.0
1.0
**
*
***
Macaque
D
Regular
Noise
Image
Density
250
500
ISI (ms)
E
Cumulative density
250
500
ISI (ms)
F
Rythmicity index
6.5
5.5
4.5
3.5
1.0
C
G
***
*
***
*
***

Figure 2

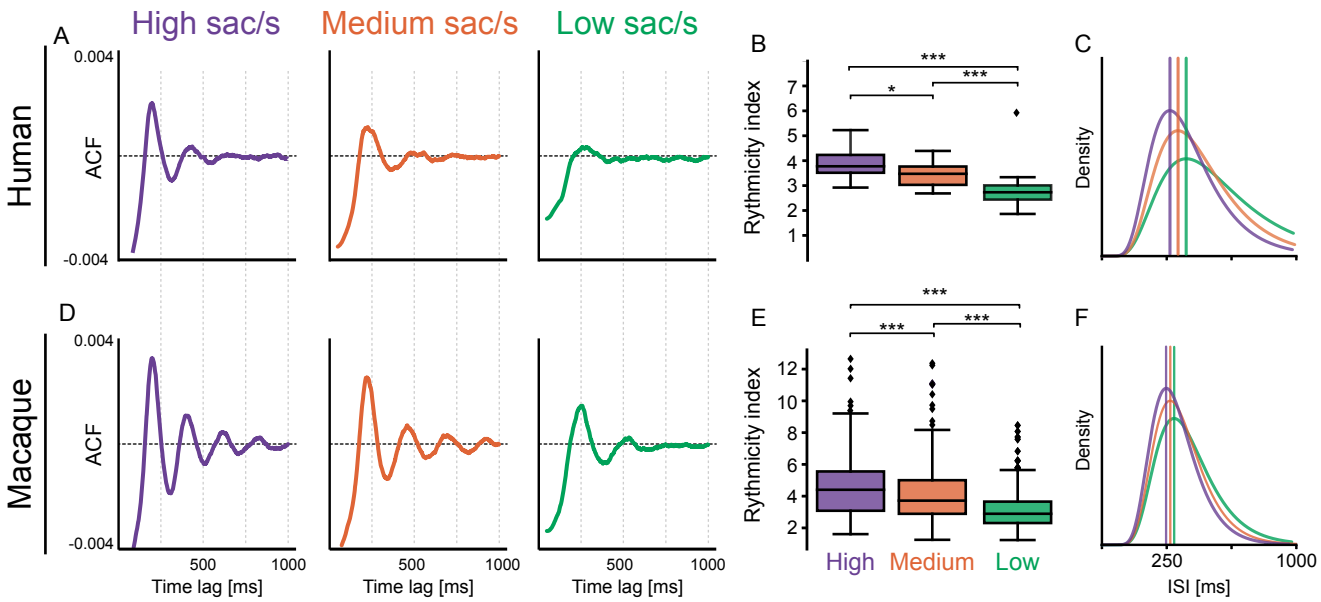
A
High sac/s
Medium sac/s
Low sac/s
Human
ACF
0.004
-0.004
500
1000
Time lag [ms]
B
Rythmicity index
***
*
C
Density
D
Macaque
E
High
Medium
Low
F
250
ISI [ms]

Figure 3

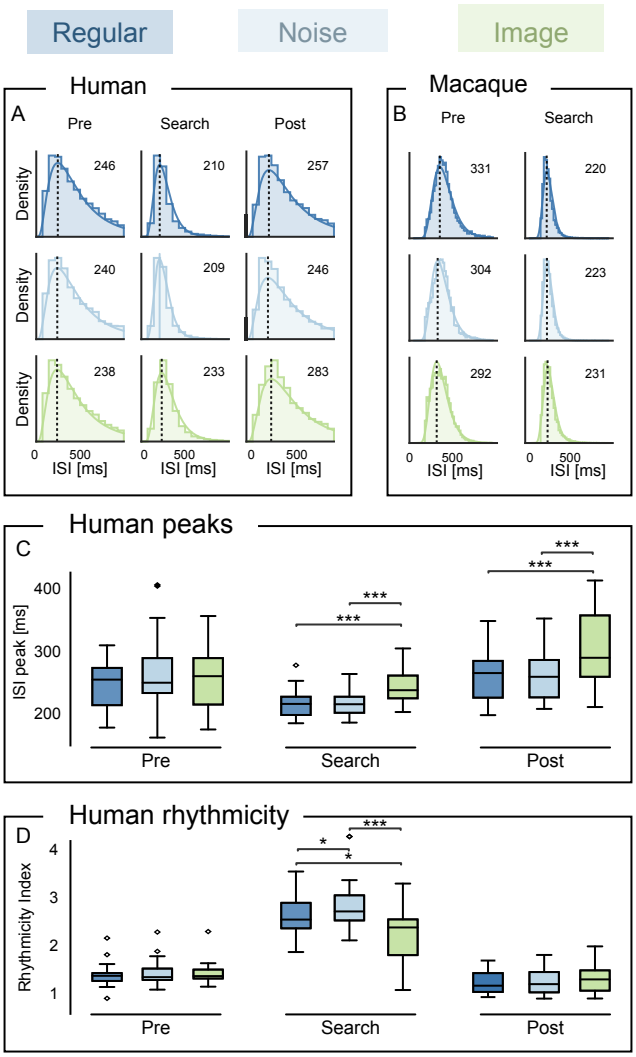
Regular
Noise
Image
Human
A
Pre
Search
Post
Density
246
210
257
240
209
246
238
233
283
0
500
ISI [ms]
Macaque
B
331
220
304
223
292
231
Human peaks
C
ISI peak [ms]
400
300
200
***
Human rhythmicity
D
Rhythmicity Index
4
3
2
1
*

Figure 4

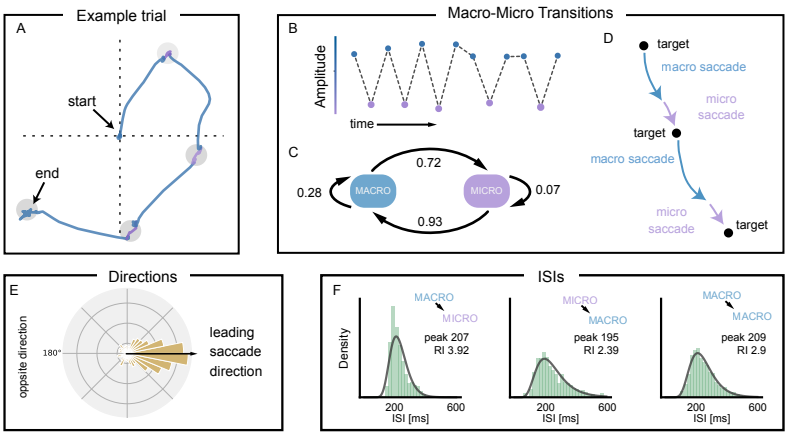
Example trial
A
start
end
Macro-Micro Transitions
B
Amplitude
time
C
0.72
0.28
MACRO
MICRO
0.07
0.93
D
target
macro saccade
micro
saccade
target
macro saccade
micro
saccade
target
Directions
E
oppsite direction
180°
leading
saccade
direction
ISIs
F
Density
MACRO
MICRO
peak 207
RI 3.92
200
600
ISI [ms]
MICRO
MACRO
peak 195
RI 2.39
200
600
ISI [ms]
MACRO
MACRO
peak 209
RI 2.9
200
600
ISI [ms]

Figure 5

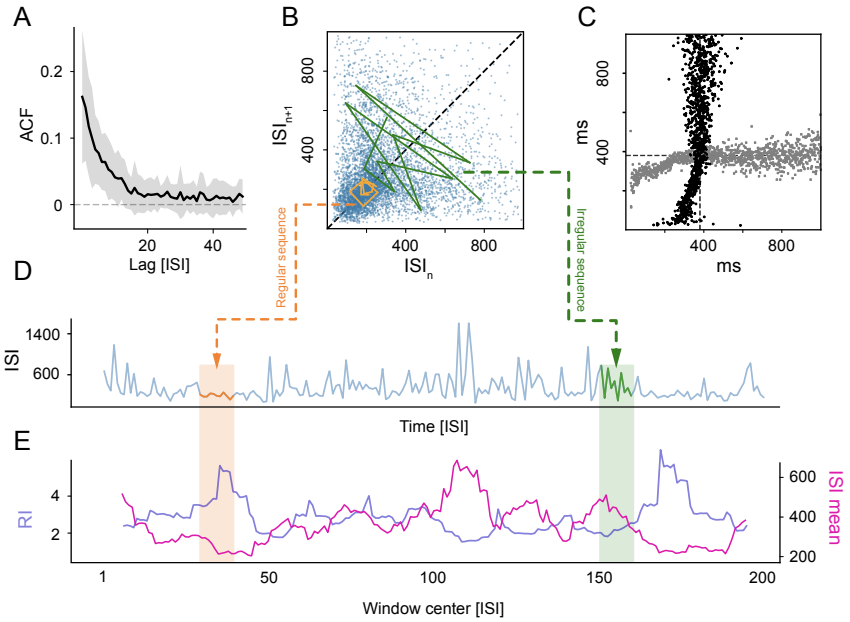
A
ACF
0.2
0.1
0
20
40
Lag [ISI]
B
ISI$_{n+1}$
800
400
400
800
ISI$_n$
Regular sequence
Irregular sequence
C
ms
800
400
400
800
ms
D
ISI
1400
600
Time [ISI]
E
RI
4
2
600
400
200
ISI mean
1
50
100
150
200
Window center [ISI]

Supplementary Figure 1

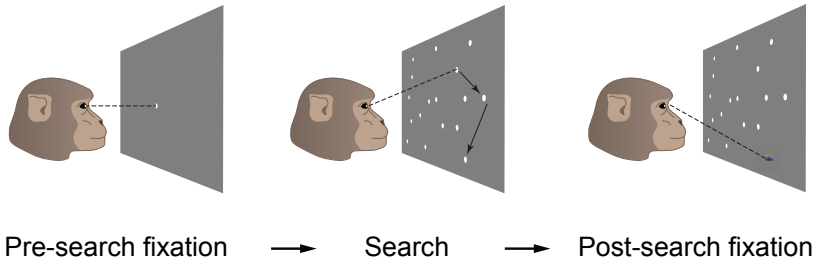

Supplementary Figure 2

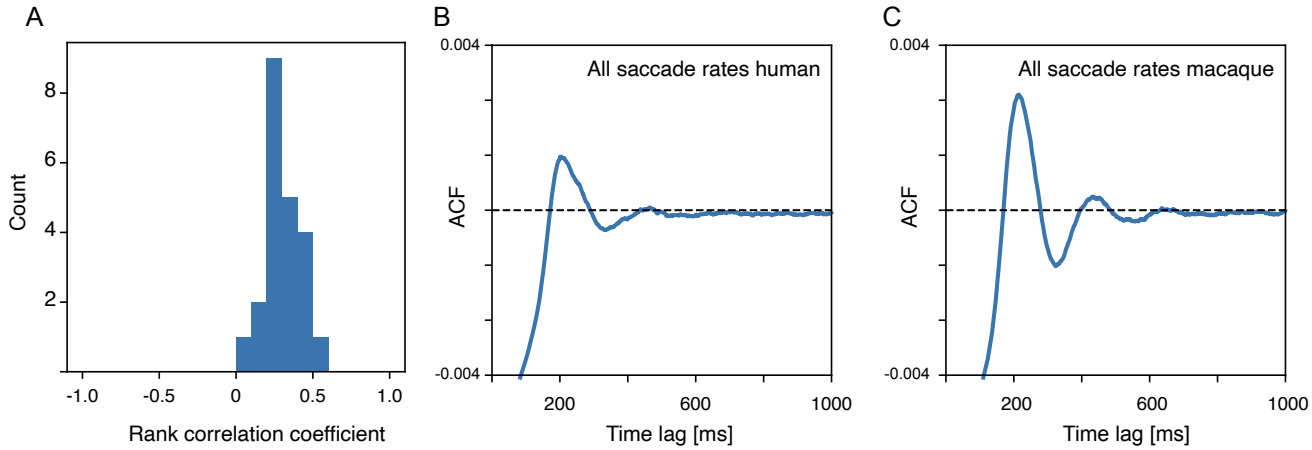

Supplementary Figure 3

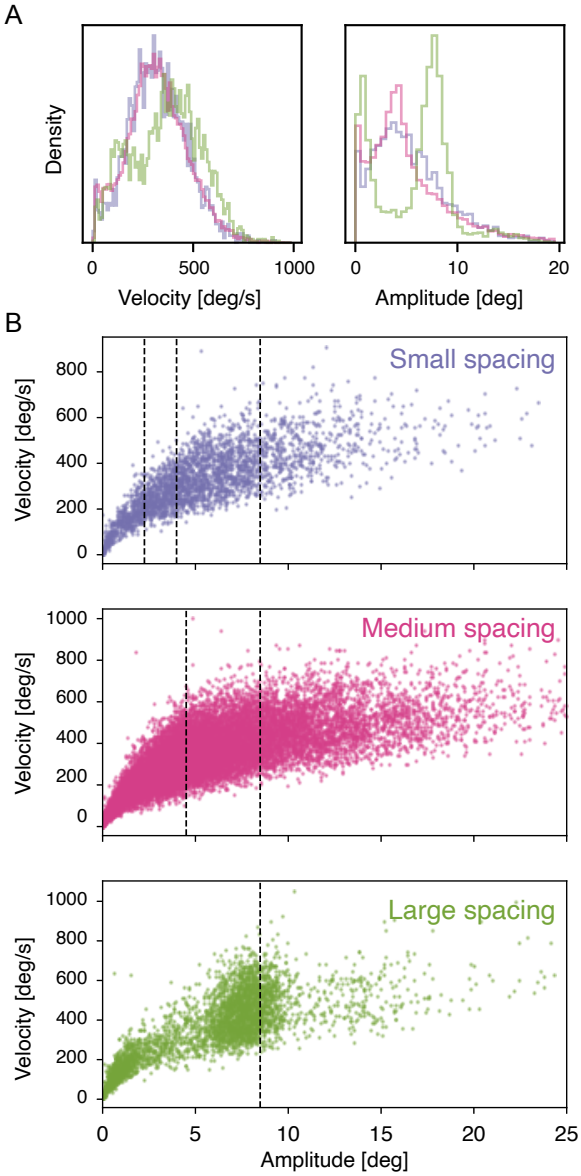
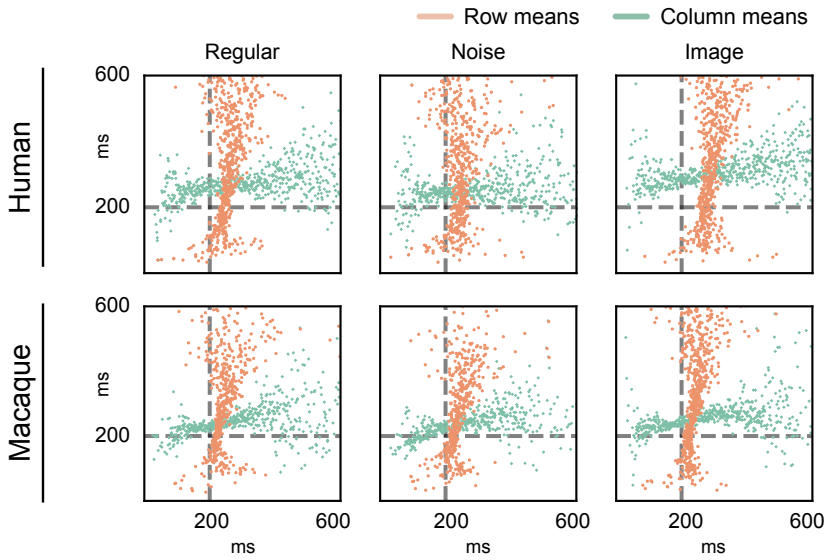
Supplementary Figure 4